Mobility-Aware Interference-Coupled ISAC for Energy-Efficient Multi-Vehicle Tracking

Atefeh Rezaei
School of Electrical Engineering and Computer Science
TU Berlin
Berlin, Germany
rezaei@ccs-labs.org

Mathis Carl
School of Electrical Engineering and Computer Science
TU Berlin
Berlin, Germany
m.carl@campus.tu-berlin.de

Falko Dressler
School of Electrical Engineering and Computer Science
TU Berlin
Berlin, Germany
dressler@ccs-labs.org

***Abstract*—Integrated sensing and communications (ISAC) has emerged as a promising technology for future vehicular networks by enabling simultaneous wireless communication and environmental sensing using shared spectrum and hardware resources. However, realizing energy-efficient multi-vehicle operation in millimeter wave (mmWave) environments remains challenging due to high mobility, inter-vehicle interference, and the strong coupling between sensing and communication performance. In this paper, we propose a mobility-aware interference-coupled ISAC framework for multi-vehicle tracking in mmWave vehicle-to-infrastructure networks. Accurate sensing and tracking of vehicle states enables efficient predictive beamforming, while the associated transmit power allocation is jointly optimized for energy efficiency under communication quality-of-service and sensing reliability requirements. To accurately capture dense vehicular deployments, inter-vehicle interference is explicitly modeled in both radar sensing and communication links, resulting in a non-convex fractional optimization problem. An efficient alternating optimization framework combining Dinkelbach's method and successive convex approximation is developed to solve the resulting problem with manageable computational complexity. Simulation results demonstrate that the proposed framework substantially improves energy efficiency while maintaining accurate multi-vehicle tracking under realistic interference conditions. Compared with existing predictive beamforming approaches, the proposed scheme achieves higher average energy efficiency and robust tracking performance across varying traffic densities, mobility levels, and noise conditions. Furthermore, the results reveal a fundamental trade-off between sensing reliability and energy efficiency that becomes increasingly pronounced in dense vehicular scenarios, highlighting the importance of interference-aware resource optimization for next-generation ISAC-enabled transportation systems.**

***Index Terms*—Integrated sensing and communication, ISAC, energy efficiency, mmWave, multi-vehicle tracking, interference-awareness**

I. Introduction

The coexistence of sensing and communication in future wireless networks offers a pathway beyond traditional spectrum partitioning. Integrated sensing and communications (ISAC) unifies these functions within a single hardware and frequency framework, eliminating redundant components and unlocking new degrees of freedom in resource utilization [1]. These features are particularly valuable in vehicular environments, where infrastructure must simultaneously support high-rate communication and accurate vehicle sensing, enabling applications such as cooperative perception, collision avoidance, and real-time traffic awareness. In this context, dual-functional radar and communication (DFRC), a prominent class of ISAC, enables roadside infrastructure to communicate with vehicles while continuously tracking their positions and velocities using the same transmission [2].

The wide bandwidth and high spatial resolution enabled by millimeter wave (mmWave) and massive multiple-input multiple-output (MIMO) technologies allow DFRC systems to simultaneously achieve precise positioning and high-rate communication [3]. Commercial interest in mmWave has grown significantly during fifth generation (5G) new radio (NR) standardization and continues to expand as sixth generation (6G) takes shape. 5G NR relies on periodic pilot transmissions and uplink feedback for channel state information (CSI) estimation, which incurs significant signaling overhead. In contrast, sensing-assisted beam tracking has emerged as a promising alternative that enables accurate beam prediction with reduced pilot signaling [4].

In this work, we propose a mobility-aware interference-coupled ISAC framework for multi-vehicle tracking in mmWave vehicle-to-infrastructure networks. Accurate sensing and tracking of vehicle states enables efficient predictive beamforming, while the associated transmit power allocation is jointly optimized for energy efficiency under communication quality of service (QoS) and sensing reliability constraints. Because transmit power directly governs the achievable sensing signal-to-interference-plus-noise ratio (SINR), the resulting power optimization in turn influences tracking accuracy, revealing a closed-loop coupling between sensing performance and energy-efficient resource allocation. Existing ISAC vehicular systems typically treat energy efficiency (EE), sensing accuracy, and communication performance as separable design objectives [5], [6], [7]. However, in dense mmWave vehicular environments, inter-vehicle interference creates a tightly coupled system where sensing quality and communication efficiency jointly degrade in a non-linear and mobility-dependent manner. This paper studies and quantifies this coupling. The proposed framework is further evaluated under dense deployment scenarios to characterize the trade-offs between EE, sensing reliability, and communication

979-8-3195-0167-7/26/$31.00 ©2026 IEEE

performance.

Our key contributions can be summarized as follows:

- We develop a system-level mobility-aware ISAC framework in which accurate multi-vehicle tracking drives predictive beamforming, coupled with an energy-efficient power allocation scheme under inter-vehicle interference; a combination absent in prior art, targeting scalable energy-efficient operation in dense and highly dynamic vehicular environments.
- We introduce an interference-aware system model that captures the impact of multi-vehicle interactions on both sensing reliability and communication performance in a unified ISAC framework.
- We propose a lightweight alternating optimization (AO) strategy for adaptive beamforming and power control in time-varying vehicular environments, designed with low computational complexity for practical deployment. The proposed method supports slot-by-slot operation, enabling adaptation to mobility-induced channel variations.
- Extensive simulation results demonstrate that the proposed framework significantly improves EE while maintaining accurate multi-vehicle tracking under interference. In addition, we provide scalability analysis under varying traffic density, mobility speed, and interference levels, and ablation studies with and without sensing constraints, highlighting the fundamental trade-off between EE and sensing reliability.

Notations: In this paper, scalars are represented by lowercase letters (e.g., a, b), vectors by bold lowercase letters (e.g., $\mathbf{h}, \mathbf{w}$), and matrices by bold uppercase letters (e.g., $\mathbf{H}, \mathbf{W}$). The superscripts $(\cdot)^T$ and $(\cdot)^H$ indicate the transpose and conjugate transpose (Hermitian), respectively. The magnitude of a scalar or vector is denoted by $|\cdot|$. The partial derivative of a scalar or vector function a with respect to b is denoted by $\frac{\partial a}{\partial b}$. The expectation operator denoted by $\mathbb{E}[\cdot]$ is used to indicate statistical averaging, e.g., in SINR expressions.

II. Related Work

A representative work in predictive beamforming is [5], which introduces a DFRC-based framework where a roadside unit (RSU) operates as a monostatic radar. Its key contribution is supporting multi-vehicle tracking, unlike single-vehicle approaches. However, it does not account for inter-vehicle interference, which becomes critical in dense vehicular environments. Vehicle states are first estimated, and an extended Kalman filter (EKF) is used for tracking and beam prediction. A power allocation scheme is designed to balance communication rate and sensing accuracy, quantified via the posterior Cramér–Rao bound. Extensions of this framework address practical limitations by proposing adaptive beamwidth strategies to balance sensing coverage and communication throughput [4]. To better capture realistic road geometries, Meng et al. [6] propose predictive beamforming on arbitrarily shaped roads using a curvilinear coordinate system combined with EKF-based tracking. Although this approach improves trajectory prediction, it is limited to single-target tracking and does not consider multi-user interference. In contrast, Liu and Masouros [7] adopt a state-model-free predictive beamforming method based on kinematic extrapolation, thereby avoiding the need for explicit state evolution models. Although robust under certain conditions, this method is sensitive to trajectory deviations and does not leverage recursive state estimation.

Table I
Comparison with prior work in ISAC-based vehicular networks.

Reference	Multi-vehicle	Interf.-aware	EE opt.	Pred. beamforming
[4], [6], [7], [8], [9], [10]	-	-	-	Yes
[5]	Yes	-	-	Yes
[11]	Yes	Yes	Yes	-
Ours	Yes	Yes	Yes	Yes

Predictive beamforming in ISAC systems has also been explored using machine learning. Wang et al. [8] jointly optimize sensing and communication via deep learning without explicit state-space modeling. Similarly, Kama et al. [9] demonstrate pilot-free predictive beamforming, reducing overhead in beam alignment and motivating low-complexity designs for multi-vehicle ISAC frameworks. Cooperative sensing-assisted predictive beam tracking has also been proposed [10], where multiple base stations collaboratively adjust beam directions using EKF fusion.

Existing sensing-assisted beam tracking works [4], [6], [7] focus on single-vehicle scenarios, whereas Liu et al. [5] consider multiple vehicles but does not account for inter-vehicle interference. Moreover, the performance metrics in prior works primarily focus on data rate or the Cramér-Rao bound (CRB), whereas EE is a key optimization metric in ISAC systems, capturing the trade-off between achievable data rate and power consumption [11], [12]. Existing ISAC frameworks optimize either predictive tracking or EE, but none jointly address both while accounting for vehicle dynamics and sensing accuracy, including both strong sensing quality assurance and EE. For instance, Liu et al. [5] consider CRB minimization and communication signal-to-noise ratio (SNR), but does not incorporate interference into the system model, which can substantially alter the underlying relationships, mathematical derivations, and resulting performance metrics. On the other side, He et al. [11] investigate EE optimization for static targets, where the sensing requirements are characterized by individual radar beampattern gain. Pursuing both objectives simultaneously becomes even more challenging in multi-vehicle scenarios where inter-vehicle interference is present.

As shown in Table I, our framework uniquely combines EE optimization with predictive power allocation in an interference-coupled multi-vehicle ISAC system. Existing ISAC frameworks typically focus on simplified system settings and are often evaluated under limited system scales, considering only a small number of vehicles and moderate mobility conditions. As a result, critical aspects such as scalability to dense multi-

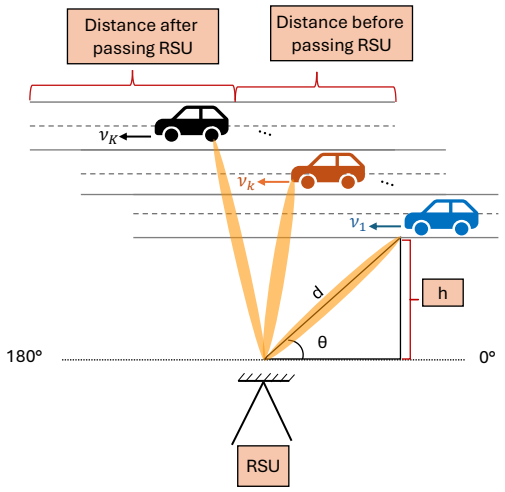


Figure 1. System model of the proposed ISAC-based tracking approach

vehicle deployments, high-mobility dynamics, and system-level trade-offs between EE, communication performance, and sensing reliability remain insufficiently explored. These limitations become particularly important in realistic vehicular environments, where traffic density and mobility significantly affect interference levels and overall system behavior.

III. System Model

We consider an ISAC-enabled RSU that provides downlink communication services to K vehicles while simultaneously sensing and tracking them, as illustrated in Figure 1. The RSU can simultaneously communicate with and sense the vehicles using the same waveform. We assume that the RSU is located at the origin of the Cartesian coordinate system and is equipped with N_T transmitting arrays, which equals the number of receiving arrays N_R. The considered scenario covers a road section consisting of 3 parallel road lanes in which every vehicle is running in a separate road lane. As visualized in Figure 1, the RSU is positioned at an orthogonal distance h from the centerline of the first road lane. Each additional road lane, running parallel to its neighboring lanes, is spaced at a distance of 2.75 m. This value corresponds to the minimum lane width specified by German road traffic licensing regulations. Each vehicle travels at a distinct velocity ν_k.

The total frame duration is divided into N time slots, each of duration T. During time slot n, the RSU transmits signals to the vehicles using the predicted beamforming from time slot $n-1$ while simultaneously receiving the echo signals with the corresponding predicted receive beamforming. From these received echoes, the RSU estimates the current vehicle states at the n-th time slot, including the angle, distance, velocity, and reflection coefficient relative to the RSU, collectively represented by the state vector $\mathbf{x}_{k,n} = [\theta_{k,n}, d_{k,n}, \nu_{k,n}, \beta_{k,n}]$. Subsequently, based on the state evolution model described in [5] and the received signal measurements processed using the matched filter and multiple signal classification (MUSIC) algorithms, an EKF is employed to refine the state estimates and predict future states, thereby enabling continuous tracking of each vehicle.

The proposed framework focuses on energy-efficient predictive beamforming. To evaluate the sensing capability enabled by the optimized beam design, we employ a conventional tracking pipeline similar to [5]. Specifically, the received sensing signal is processed using the well-known MUSIC algorithm to obtain angle of arrival (AoA) measurements, which are then used by a standard EKF to estimate and predict vehicle states. The resulting state predictions are used to steer the sensing and communication beams in the subsequent time slot. Since MUSIC and EKF are adopted as standard benchmark components, we omit their detailed derivation and focus instead on how the proposed energy-efficient beamforming framework influences sensing SINR and, consequently, tracking performance.

Finally, based on the estimated states at the current time slot and the state evolution model on the vehicle mobility behavior, which provides one-step prediction, we predict the vehicle's next state, $\mathbf{x}_{k,n+1|n}$, to enable predictive beamforming in the following time slot, $n+1$ [5].

A. Radar Model

The RSU emits several narrow beams towards the direction of the vehicles and extracts the desired sensing information from the received echo signals. The transmitted signal from the RSU at time instant t of the n-th time slot for vehicle k is denoted by $s_{k,n}(t)$. The transmit and received steering vector of the uniform linear array (ULA) of the RSU in the direction of vehicle k is given by

$$\mathbf{a}(\theta_{k,n}) = \sqrt{\frac{1}{N_T}}\left[1, e^{-j2\pi\frac{\hat{d}}{\tilde{\lambda}}\cos(\theta_{k,n})}, ..., e^{-j2\pi\frac{\hat{d}}{\tilde{\lambda}}(N_T-1)\cos(\theta_{k,n})}\right]^T, \quad (1)$$

where $\theta_{k,n}$ is the angle of departure corresponding to vehicle k, $\tilde{\lambda}$ is the carrier wavelength, and $\hat{d}$ denotes the spacing between two adjacent antennas. The received signal at the RSU side can be described using the radar signal model, considering the Doppler shift ($\mu_{k,n}$) and the propagation delay ($\tau_{k,n}$). We also take into account interference caused by echoes from the i-th vehicle. We assume the transmit beamforming vector, i.e., $\boldsymbol{f}_{\text{Tx},k,n} = \boldsymbol{a}(\hat{\theta}_{k,n|n-1})$. Hence, the echo signal received at the RSU in time slot n after filtering of the other unwanted directions is given by

$$r_{k,n} = \kappa \sum_{i=1}^{K} \Big(\sqrt{p_{i,n}}\beta_{i,n} e^{j2\pi\mu_{i,n}t} \boldsymbol{f}_{\text{Rx},k,n}^H \boldsymbol{a}(\theta_{k,n}) \boldsymbol{a}^H(\theta_{k,n}) \boldsymbol{f}_{\text{Tx},i,n} s_{i,n}(t-\tau_{i,n}) \Big) + z_s(t), \quad (2)$$

where $z_s(t)$ denotes the additive white Gaussian noise (AWGN) at the RSU, $p_{i,n}$ is the transmit power of vehicle i, and $\beta_{k,n}$ represents the reflection coefficient. Furthermore, $\kappa = \sqrt{N_T N_R}$ denotes the antenna array gain. We assume the received beamforming $\boldsymbol{f}_{\text{Rx},k,n}$, to limit the caused interference from the other targets rather than the k-th target, resulting in a

higher SNR and more accurate vehicle state estimations. To ensure adequate sensing performance, the sensing SINR of vehicle k at time slot n is required to exceed a predefined threshold ϵ_{R}. The sensing SINR ($\Gamma_{k,n}^{\text{radar}}$) is calculated as in (3), where $\boldsymbol{A}(\theta_{k,n}) = \boldsymbol{a}(\theta_{k,n})\boldsymbol{a}^T(\theta_{k,n})$.

B. Energy Efficiency

Based on the communication model, the received signal at vehicle k in time slot n is described as

$$\begin{aligned} &q_{k,n}(t) = \\ &\tilde{\kappa}\sqrt{p_{k,n}}\,\alpha_{k,n}\,e^{j2\pi\mu_{k,n}t}\,\boldsymbol{a}^H(\theta_{k,n})\,\boldsymbol{f}_{Tx,k,n}\,s_{k,n}(t) + z_c(t) \\ &+ \tilde{\kappa}\sum_{\substack{i=1\\ i\neq k}}^{K}\sqrt{p_{i,n}}\,\alpha_{k,n}\,e^{j2\pi\mu_{k,n}t}\,\boldsymbol{a}^H(\theta_{k,n})\,\boldsymbol{f}_{Tx,i,n}\,s_{i,n}(t), \end{aligned} \quad (4)$$

where $\tilde{\kappa} = \sqrt{N_T}$ and

$$\alpha_{k,n} = \tilde{\alpha}\,d_{k,n}^{-1}\,e^{j\frac{2\pi}{\lambda}d_{k,n}} = \tilde{\alpha}\,d_{k,n}^{-1}\,e^{j\frac{2\pi f_c}{c}d_{k,n}} \quad (5)$$

and $z_c(t) \sim \mathcal{CN}(0,\sigma_c^2)$ is the AWGN noise at vehicle k. Consequently, the received SINR of vehicle k in time slot n is given by

$$\gamma_{k,n}^{\text{com}} = \frac{p_{k,n}\left|\tilde{\kappa}\alpha_{k,n}\boldsymbol{a}^H(\theta_{k,n})\boldsymbol{f}_{Tx,k,n}\right|^2}{\sum_{\substack{i=1\\ i\neq k}}^{K} p_{i,n}\left|\tilde{\kappa}\alpha_{k,n}\boldsymbol{a}^H(\theta_{k,n})\boldsymbol{f}_{Tx,i,n}\right|^2 + \sigma_c^2} \quad (6)$$

The EE is expressed as the ratio between the total achievable data rate and the total power consumption. Following standard practice in EE optimization, we express the data rate in terms of spectral efficiency (bits/s/Hz) to obtain a bandwidth-independent metric. The data rate is typically determined according to Shannon's capacity formula, which specifies the theoretical upper limit of the achievable data rate. Thus, the spectral efficiency is calculated as

$$\eta_{SE} = \sum_{k=1}^{K}\log_2(1+\gamma_{k,n}^{\text{com}}). \quad (7)$$

The total power consumption, which includes static and dynamic power consumptions for the RSU, is described as

$$P_{\text{total}} = P_{\text{static}} + N_{\text{T}}P_{\text{RFchain}} + \frac{1}{\zeta}\sum_{k=1}^{K}p_{k,n}, \quad (8)$$

where P_{total} denotes the total power consumption of the considered system. The static component, P_{static}, represents fixed power requirements, such as those for cooling systems or power supply losses, and does not depend on any optimization variables like $p_{k,n}$. Note that P_{total}, P_{static}, P_{RFchain}, and $p_{k,n}$ in (8) are expressed in linear scale (W); the corresponding values reported in Table II are given in dBm for convenience and are converted via $P_{[\text{mW}]} = 10^{P_{[\text{dBm}]}/10}$ prior to use in the optimization. Following [13], [14], P_{static} is assigned a constant value of 30 dBm. The dynamic part of the power consumption accounts for both the RF chain-related power, P_{RFchain}, and the transmit power, $\sum_{k=1}^{K}p_{k,n}$. P_{RFchain} represents the power required by hardware components such as signal processors, A/D converters, and power amplifiers for a single RF chain. Since these values are determined by hardware specifications, P_{RFchain} is treated as a fixed quantity (20 dBm, following [13], [14]), and is multiplied by N_{Antenna}, which corresponds to the number of transmitting and receiving antennas at the RSU (N_T and N_R in this work). The transmit powers $p_{k,n}$, in contrast, are the optimization variables. Finally, the power amplifier efficiency ζ is introduced to account for the conversion losses between input electrical power and radiated RF power [15].

IV. Energy Efficiency Optimization

A. Problem Formulation

We aim to maximize the EE for information transmission and sensing while guaranteeing the QoS of the communication service and the sensing which leads to more accurate localization and tracking. The optimization problem is mathematically formulated as

$$\begin{aligned} \mathcal{P}_1 : &\max_{p_{k,n}} \mathcal{O}bj_1 \triangleq \frac{\sum_{k=1}^{K}\log_2(1+\gamma_{k,n}^{\text{com}})}{P_{\text{total}}} \\ \text{s.t.}\quad &\text{C1} : \Gamma_{k,n}^{\text{radar}} \geq \epsilon_{\text{R}}, \quad \forall k,n, \\ &\text{C2} : \sum_{k=1}^{K}p_{k,n} \leq P_{\text{budget}}, \quad \forall n, \\ &\text{C3} : p_{k,n} > 0, \quad \forall k,n. \end{aligned} \quad (9)$$

In $\mathcal{P}_1$, $p_{k,n}$ is the transmit power for the k-th vehicle as an optimization variable. Constraint C1 guarantees sensing accuracy in the presence of interference by imposing a sensing SINR requirement for each individual vehicle at every time slot. Constraint C2 limits the transmit power of the RSU, where P_{budget} denotes the maximum allowable transmit power. Constraint C3 ensures that the allocated power is valid and non-negative.

B. Solution of the Optimization Problem

In general, the optimization problem $\mathcal{P}_1$ is non-convex and nonlinear due to the non-convexity of its objective function. It can be observed that the formulated objective function has a fractional structure, which renders the problem non-convex and motivates the use of the Dinkelbach algorithm for its solution [16]. Accordingly, the objective can be expressed as the ratio of two functions, denoted by $L(p_{k,n})$ and $D(p_{k,n})$ as

$$\max_{p_{k,n}}\left[\frac{L(p_{k,n})}{D(p_{k,n})}\right] \quad (10)$$

where $L(p_{k,n}) = \sum_{k=1}^{K}\log_2(1+\gamma_{k,n}^{\text{com}})$ and $D(p_{k,n}) = P_{\text{total}}$. We define the objective function in (10) as λ_n^* Within the solution algorithm, λ^j denotes the obtained value at the j-th iteration of the Dinkelbach method, and λ_n^* represents the globally optimal value of the objective function in the current time slot n, achieved by the sub-optimal power allocation $p_{k,n}$.

The fractional objective function can be reformulated using the Dinkelbach method as

$$\max_{p_{k,n}} \mathcal{O}bj_2 \triangleq L(p_{k,n}) - \lambda_n\,D(p_{k,n}), \quad (11)$$

$$\Gamma_{k,n}^{\text{radar}} = \frac{\mathbb{E}\left[\left|\kappa\sqrt{p_{k,n}}\beta_{k,n}e^{j2\pi\mu_{k,n}t}\boldsymbol{f}_{\text{Rx},k,n}^H\boldsymbol{A}(\theta_{k,n})\boldsymbol{f}_{\text{Tx},k,n}s_{k,n}(t-\tau_{k,n})\right|^2\right]}{\sum_{\substack{i=1\\i\neq k}}^{K}\mathbb{E}\left[\left|\kappa\sqrt{p_{i,n}}\beta_{i,n}e^{j2\pi\mu_{i,n}t}\boldsymbol{f}_{\text{Rx},k,n}^H\boldsymbol{A}(\theta_{k,n})\boldsymbol{f}_{\text{Tx},i,n}s_{i,n}(t-\tau_{i,n})\right|^2\right]+\mathbb{E}[|z_s(t)|^2]}$$

$$= \frac{p_{k,n}\left|\beta_{k,n}\boldsymbol{f}_{\text{Rx},k,n}^H\boldsymbol{A}(\theta_{k,n})\boldsymbol{f}_{\text{Tx},k,n}\right|^2}{\sum_{\substack{i=1\\i\neq k}}^{K}p_{i,n}\left|\beta_{i,n}\boldsymbol{f}_{\text{Rx},k,n}^H\boldsymbol{A}(\theta_{k,n})\boldsymbol{f}_{\text{Tx},i,n}\right|^2+\sigma_s^2} \tag{3}$$

where λ_n is the Dinkelbach parameter updated iteratively until convergence. The objective function $\mathcal{O}bj_2$ remains non-convex due to the intrinsic non-convexity of the data rate function. To address this issue, we express the rate function in a difference-of-convex (DC) form and solve it using the successive convex approximation (SCA) algorithm as

$$\begin{aligned}R_{k,n} &= \log_2(1+\gamma_{k,n}^{\text{com}})\\ &= \underbrace{\log_2\left(\sum_{i=1}^{K}p_{i,n}\left|\tilde{\kappa}\,\alpha_{k,n}\,\boldsymbol{a}^H(\theta_{k,n})\,\boldsymbol{f}_{Tx,i,n}\right|^2+\sigma_c^2\right)}_{w_{k,n}}\\ &\quad\underbrace{-\log_2\left(\sum_{\substack{i=1\\i\neq k}}^{K}p_{i,n}\left|\tilde{\kappa}\,\alpha_{k,n}\,\boldsymbol{a}^H(\theta_{k,n})\,\boldsymbol{f}_{Tx,i,n}\right|^2+\sigma_c^2\right)}_{g_{k,n}}\\ &= w_{k,n}(p_{k,n})-g_{k,n}(p_{k,n}).\end{aligned} \tag{12}$$

Both sub-functions, $w_{k,n}$ and $g_{k,n}$, are concave with respect to the optimization variables $p_{i,n}$. Employing the DC approximation, $g_{k,n}$ is approximated as

$$\tilde{g}_{k,n}(p_{k,n}) = g_{k,n}(p_{k,n}^{(a)}) + \sum_{\substack{i=1\\i\neq k}}^{K}\frac{\partial g_{k,n}}{\partial p_{i,n}}\Big|_{\{p_{i,n}^{(a)}\}}\left(p_{i,n}-p_{i,n}^{(a)}\right) \tag{13}$$

where

$$\frac{\partial g_{k,n}}{\partial p_{i,n}}\Big|_{\{p_{i,n}^{(a)}\}} = \frac{1}{\ln(2)}\cdot\frac{|C_{k,n}|^2}{p_{i,n}^{(a)}|C_{k,n,i}|^2+\sigma_c^2} \tag{14}$$

$$C_{k,n} = \tilde{\kappa}\cdot\alpha_{k,n}\cdot\boldsymbol{a}^H(\theta_{k,n})\cdot\boldsymbol{f}_{Tx,i,n} \tag{15}$$

in which a is the SCA iteration index. After applying a sequence of convex approximations, problem $\mathcal{P}_1$ can be reformulated as

$$\begin{aligned}&\mathcal{P}_2: \max_{p_{k,n}}\mathcal{O}bj_3 \triangleq w_{k,n}-\tilde{g}_{k,n}-\lambda_n D_{k,n},\\ \text{s.t.}\quad &\text{C2, C3}:\\ &\text{C1}: \left|\beta_{k,n}\boldsymbol{f}_{\text{Rx},k,n}^H\boldsymbol{A}(\theta_{k,n})\boldsymbol{f}_{\text{Tx},k,n}\right|^2 p_{k,n}-\\ &\epsilon_{\text{R}}\sum_{\substack{i=1\\i\neq k}}^{K}p_{i,n}\left|\beta_{i,n}\boldsymbol{f}_{\text{Rx},k,n}^H\boldsymbol{A}(\theta_{k,n})\boldsymbol{f}_{\text{Tx},i,n}\right|^2 \geq \epsilon_{\text{R}}\sigma_s^2 \quad \forall k,n,\end{aligned}$$

which is convex and can be efficiently solved using the proposed AO-based solution summarized in Algorithm 1. In the inner loop, the SCA method iteratively solves a sequence of convex subproblems constructed from the approximated rate function. The iterations continue until the normalized difference between the objective function values of two consecutive iterations falls below a predefined threshold δ_{SCA}, at which point the SCA loop terminates, yielding a locally optimal solution. In the outer loop, the Dinkelbach algorithm updates the auxiliary parameter λ_n based on the obtained SCA solution and evaluates the fractional optimality condition using the convergence threshold $\delta_{\text{Dinkelbach}}$, repeating the process until convergence.

Algorithm 1 Solving the optimization problem via Dinkelbach and SCA

Require: Set initialized power $p_{k,n}^{(0)}$ and convergence accuracy δ_{SCA}.

$\lambda_n^{(0)} \leftarrow \frac{L(p_{k,n}^{(0)})}{D(p_{k,n}^{(0)})}$
$j \leftarrow 1$
while not converged **do**
  Set $a \leftarrow 1$
  while not converged **do**
    Calculate $\tilde{g}_{k,n}(p_{k,n}^{(a)})$
    Solve $\mathcal{P}_2$
    if $\frac{|\mathcal{O}bj_1(p_{k,n}^{(a)})-\mathcal{O}bj_1(p_{k,n}^{(a-1)})|}{\max\{\mathcal{O}bj_1(p_{k,n}^{(a)}),\,\mathcal{O}bj_1(p_{k,n}^{(a-1)})\}} < \delta_{\text{SCA}}$ **then**
      Update $p_{k,n}$ in the Dinkelbach approach
      break
    else
      $a \leftarrow a+1$
    end if
  end while
  Solve problem $\mathcal{P}_2$ for a given $\lambda_n^{(j-1)}$
  if $|w^{(j)}-\tilde{g}^{(j)}-\lambda_n^{(j-1)}D^{(j)}| \leq \delta_{\text{Dinkelbach}}$ **then**
    return $\lambda_n^* = \lambda_n^{(j-1)}$ and $p_{k,n}^*$
  else
    $\lambda_n^{(j+1)} \leftarrow \frac{L(p_{k,n}^{(j)})}{D(p_{k,n}^{(j)})}$
    $j \leftarrow j+1$
  end if
end while

C. Convergence and Computational Complexity Analysis

Next, we analyze the proposed approach in Algorithm 1 in terms of convergence properties and computational complexity.

The convergence of the proposed algorithm follows from the monotonic improvement property of each optimization stage [17]. During each SCA iteration, the surrogate problem provides a locally tight approximation, ensuring that the objective value does not decrease between successive updates. Similarly, the alternating optimization framework sequentially optimizes individual variable blocks while keeping the remaining variables fixed, leading to non-decreasing EE values across iterations such that

$$\mathrm{EE}^{(j+1)} \geq \mathrm{EE}^{(j)}.$$

Since the Dinkelbach-based fractional programming procedure guarantees convergence under standard conditions, and the achievable EE is upper-bounded due to finite transmit power and communication resources, the objective sequence generated by the proposed algorithm converges.

Moreover, we analyze the computational complexity of Algorithm 1 based on the SCA method. The computational complexity per SCA iteration is given by $\mathcal{O}\big(\log(1/\delta_{\mathrm{SCA}})P_{\mathrm{S}}C_{\mathrm{S}}^3\big)$, where δ_{SCA} denotes the solution accuracy [18]. Here, the problem size and number of constraints are given by $P_{\mathrm{S}} = K + 1$ and $C_{\mathrm{S}} = 2K + 1$, respectively. Within each Dinkelbach iteration, this complexity corresponds to a single SCA update in one time slot. Considering I_{D} Dinkelbach iterations per slot, the per-slot computational complexity becomes $\mathcal{O}\big(I_{\mathrm{D}}\log(1/\delta_{\mathrm{SCA}})P_{\mathrm{S}}C_{\mathrm{S}}^3\big)$. Finally, for a frame consisting of N time slots, the overall complexity scales linearly with N.

V. Simulation Results

A. Simulation Platform and Parameters

The simulation platform was implemented in MATLAB R2024a using the CVX modeling framework with the MOSEK solver. At each slot, the EKF predicts vehicle states, predictive beamforming is applied, transmit powers are optimized via the proposed Dinkelbach–SCA algorithm in CVX, and MUSIC matched filtering extracts sensing parameters for the EKF update.

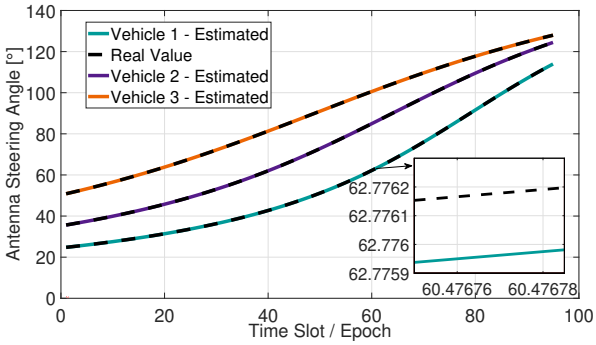
Figure 1 illustrates the system model, which consists of K vehicles. Initially, we consider a low-density setting with $K = 3$ vehicles, consistent with settings commonly used in the literature. We then evaluate the efficiency of the proposed framework under more densely populated scenarios. The vehicles start moving from the coordinates $(130, 60)$, $(86, 62.75)$, and $(52, 65.5)$ along a straight path from the right side of the RSU to the left at constant velocities of 60, 50, and 40 km/h, respectively. The y-coordinates are defined according to a lane spacing of 2.75 m between adjacent road lanes. Unless specified otherwise, we set the noise power to $\sigma_k^2 = -90$ dBm and the maximum transmit power to $P_{\mathrm{budget}} = 30$ dBm, which is the typical transmit power for mmWave case in 3GPP NR FR2 standard. The key simulation parameters are summarized in Table II.

B. AoA Estimation and Tracking Accuracy

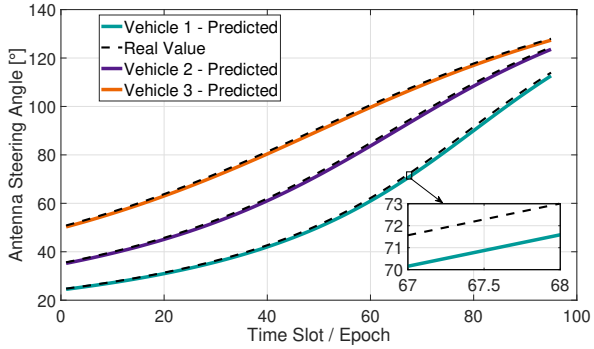
We first validate the optimization framework by evaluating its ability to achieve the required sensing and tracking accuracy.

Table II
Simulation Framework Parameters.

Symbol	Parameter	Value
N_T/N_R	Number of Tx/Rx antennas	8
T	Time slot length	0.1 s
N	Number of time slots	95
K	Number of vehicles	3
h	RSU orthogonal offset (lane 1)	60 m
A	Simulated road segment area ($K = 3$)	$\approx$0.012 km^2
f_c	Carrier frequency	60 GHz
λ	Wavelength	5 mm
P_{budget}	Transmit power budget	30 dBm
ϵ_{R}	Radar-related SINR threshold	0 dBm
σ_c^2	Communication noise	-90 dBm
σ_s^2	Sensing noise	-90 dBm
v_k	Vehicle velocities	60, 50, 40 km/h
σ_θ	Steering angle standard deviation	0.02°
σ_d	Distance standard deviation	0.2 m
σ_v	Velocity standard deviation	0.5 km/h
σ_β	Reflection coefficient standard deviation	0.1
P_{static}	Static power consumption	30 dBm
P_{RFchain}	Power consumption per RF chain	20 dBm
ζ	Power amplifier efficiency	20%
δ_{SCA}	Accuracy for the SCA approach	0.01
$\delta_{\mathrm{Dinkelbach}}$	Accuracy for the Dinkelbach approach	0.01



(a) Estimation of angle with EKF.



(b) Estimation of angle without EKF in each time slot.

Figure 2. AoA estimation accuracy for three vehicles with and without EKF.

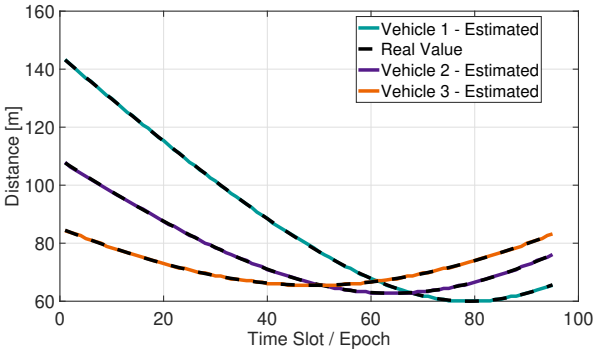


Figure 3. Range estimation accuracy for three vehicles.

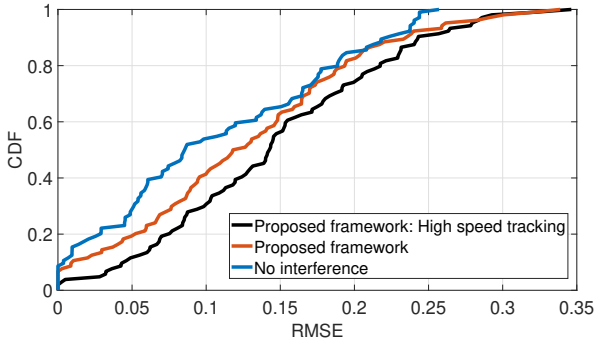


Figure 4. Range estimation accuracy analysis for different velocity scenarios ($K = 3$ and $N = 130$).

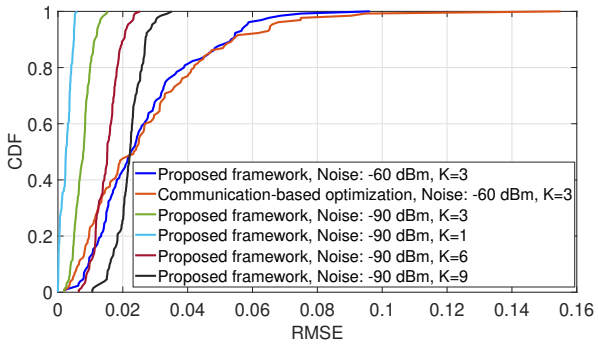


Figure 5. Angle estimation accuracy analysis under sensing and communication trade-off ($K = 3$ and $N = 130$).

Figures 2a and 2b show the AoA estimation accuracy and tracking performance of the proposed optimization framework across all time slots, following the trajectories of the three independent vehicles described in Figure 1. Figure 2a shows the angle tracking for three different vehicles, demonstrating a very high level of accuracy. In contrast, Figure 2b illustrates the case where the EKF advantages and estimation refinement are not applied at every time slot, resulting in lower tracking accuracy. Another important observation is that the estimation inaccuracy is highest for the first vehicle, who has a higher velocity and is farther from the RSU, and lowest for the third vehicle, who has a lower velocity and is closer to the RSU.

Additionally, we evaluate the range estimation accuracy for the same setup in Figure 3, confirming accurate range estimation and reliable target tracking throughout the setup. To better demonstrate the range estimation accuracy, in Figure 4, we evaluate how increased vehicle velocity (by 30 km/h) affects estimation performance. Moreover, we use [5] as a benchmark to evaluate the proposed framework. Although the benchmark in [5] achieves slightly higher sensing accuracy under the idealized assumption of interference-free operation, the proposed framework explicitly accounts for realistic inter-vehicle interference and still maintains reliable sensing and tracking performance. Furthermore, the proposed scheme attains a higher average EE of 5.7663, bits/Joule/Hz over the considered time horizon, compared with 5.1471, bits/Joule/Hz achieved by the benchmark in [5]. This indicates that the proposed optimization framework effectively mitigates the performance degradation caused by interference. Overall, the results demonstrate that the proposed interference-aware design substantially improves EE while preserving reliable sensing and tracking capabilities.

C. ISAC Trade-Off

Figure 5 evaluates the sensing accuracy of the proposed algorithm in comparison with a communication-based optimization scheme where the sensing constraint is removed. The results demonstrate that the proposed approach achieves high sensing accuracy due to the enforcement of constraint C_1. Furthermore, we examine the impact of noise power on the root mean square error (RMSE). It is evident that the RMSE under higher noise power ($\sigma_c^2 = \sigma_s^2 = -60, \text{dBm}$) is significantly worse than that under lower noise power ($\sigma_c^2 = \sigma_s^2 = -90, \text{dBm}$). The figure also validates the proposed multi-vehicle tracking approach compared with single-vehicle tracking. To assess network performance under increased traffic density and varying vehicle velocities, the total number of vehicles was increased from 3 to 9, with three vehicles assigned to each road lane. The evaluated range ($K = 3$ to 9) reflects a moderate-density scenario consistent with the 3-lane road segment considered, corresponding to approximately 16–38 vehicles/km, as detailed in Table II. Without loss of generality, the initial locations of the added vehicles are $\{(153, 60), (136, 62.78), (125, 65.5)\}$ and $\{(177, 60), (156, 62.75), (145, 65.5)\}$, with velocities $\{70, 75, 65, 85, 80, 75\}$ km/h. Moreover, we evaluate the impact of the number of vehicles on the RMSE in denser scenarios. As the number of vehicles increases from $K = 1$ to $K = 9$, the accuracy decreases.

Figure 6 shows the cumulative distribution function (CDF) of the AoA estimation RMSE for the proposed ISAC-based predictive tracking framework and a conventional 5G-NR beam management baseline under multi-vehicle mobility. The 5G-NR baseline relies on periodic beam sweeping and codebook-based beam selection without continuous sensing. Results show that the proposed scheme achieves lower RMSE across the entire

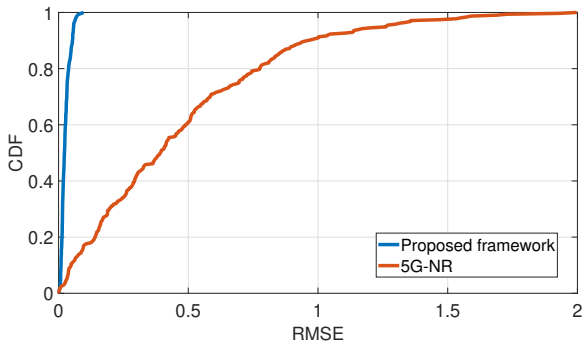


Figure 6. Angle estimation accuracy analysis for both ISAC-based estimation and tracking with 5G-NR ($K = 3$ and $N = 130$).

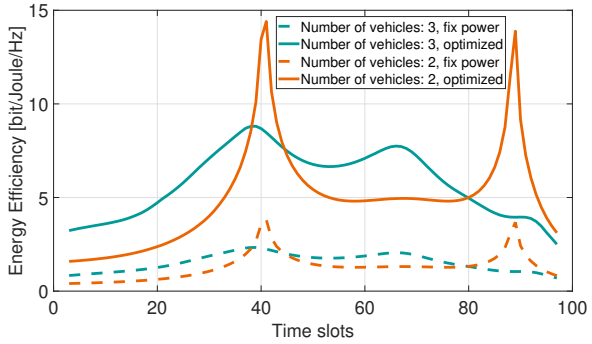


Figure 7. Energy efficiency analysis for different numbers of vehicles ($\sigma_c^2 = \sigma_s^2 = -90$dBm).

CDF range. Overall, the results demonstrate that integrating predictive sensing with beam management improves AoA estimation accuracy and reliability compared to standard 5G-NR procedures in dynamic multi-vehicle scenarios.

D. Energy Efficiency Analysis

Figure 7 illustrates the variation of overall EE for scenarios with different numbers of vehicles. A system with fixed transmit power is used as a reference to quantify the performance gains achieved through the proposed optimization approach. In

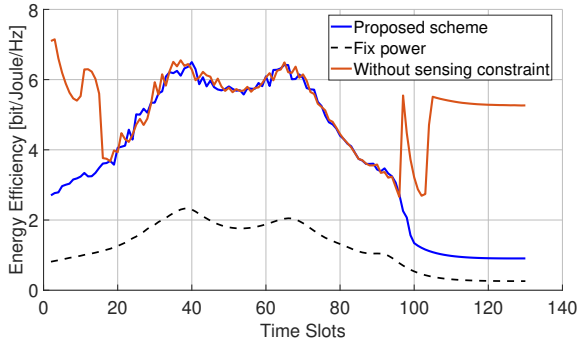


Figure 8. Energy efficiency analysis under sensing and communication trade-off ($K = 3$, $N = 130$, and $\sigma_c^2 = \sigma_s^2 = -60$dBm).

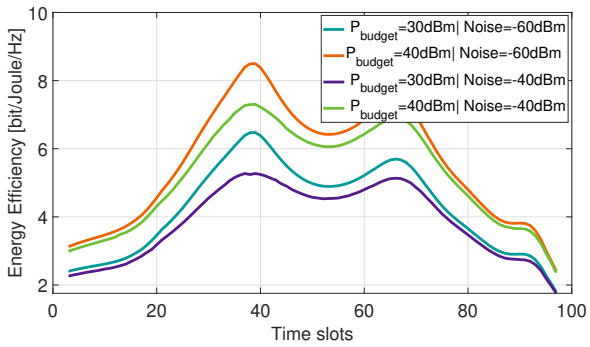


Figure 9. Energy efficiency optimization improvements compared to a fixed transmit power.

general, the two-vehicle scenario exhibits two local maxima in EE, which occur approximately when the distance between a vehicle and the RSU is minimal. This scenario considers vehicles 1 and 2 as depicted in Figure 7. Notably, the time instants at which the vehicles reach their minimum distances to the RSU do not exactly coincide with the local maxima of EE. A similar behavior is also observed in the three-vehicle scenario. This effect arises because, when multiple vehicles transmit simultaneously, the SINR of each link depends not only on its own distance to the RSU but also on the instantaneous positions of the other vehicles. Consequently, mutual interference plays a significant role in addition to distance in determining the achievable EE. At time slot 41, the maximum system EE reaches 14.4, bits/Joule/Hz, corresponding to an improvement of 10.59, bits/Joule/Hz compared to the fixed transmit power baseline. Aside from the two local maxima observed in the two-vehicle scenario, the three-vehicle scenario achieves a higher overall EE in most time slots.

Figure 8 illustrates the trade-off between sensing and communication. First, we evaluate the EE for $\sigma_c^2 = \sigma_s^2 = -60$, dBm, which exhibits greater fluctuations compared to Figure 7 under the same parameter settings. We further assess the performance trade-off between the proposed framework and a benchmark scheme based solely on communication optimization, where the sensing quality constraint is removed. The results indicate that when the vehicle is closer to the RSU, the difference in achieved EE between the two approaches is negligible. However, as the distance between the Vehicles and the RSU increases, the EE achieved by the communication-only optimization becomes higher than that of the scheme incorporating stringent sensing quality requirements. This observation highlights the inherent trade-off between sensing and communication, particularly in long-distance scenarios.

Figure 9 depicts the EE gains obtained by the proposed optimization scheme in the case of three vehicles. To highlight the benefits of the optimization, the difference in total EE between the optimized system and the fixed transmit power baseline is computed and visualized. Moreover, multiple transmit power budget values are considered to demonstrate their joint impact with noise power on the system performance. The largest

improvement is observed under a transmit power budget of 40 dBm and a noise power of -60 dBm, where the maximum gain reaches 8.49 bits/Joule/Hz. For all simulation parameters listed in Table II, the algorithm consistently converges within 25 SCA iterations per time slot. The outer Dinkelbach loop typically converges within 3–5 iterations.

VI. Conclusion

We proposed a multi-vehicle ISAC framework that jointly optimizes energy efficiency, sensing accuracy, and communication performance in mobile networks. Leveraging high-accuracy signal processing techniques (MUSIC, matched filter, and EKF), the framework tracks and localizes multiple vehicles while accounting for interference in both communication and sensing channels. We formulated a non-convex fractional program and developed an alternating optimization algorithm combining Dinkelbach and SCA. Simulation results demonstrate that the proposed scheme enhances EE and sensing accuracy simultaneously, enabling reliable multi-vehicle tracking under interference across scenarios with varying numbers of vehicles. Future work includes extending the framework to full-duplex operation and non-line-of-sight scenarios, as well as reducing algorithm complexity for real-time deployment.

Acknowledgments

This work was supported by the Federal Ministry of Research, Technology, and Space (BMFTR, Germany) within the project xG-RIC under grant 16KIS2429K as well as by the German Research Foundation (DFG) within the project RADCOM-HETNET under grant DR 639/18-4.

References

[1] H. Wymeersch et al., "Integration of Communication and Sensing in 6G: a Joint Industrial and Academic Perspective," in *IEEE International Symposium on Personal, Indoor and Mobile Radio Communications (PIMRC 2021)*, Virtual Conference: IEEE, Sep. 2021, pp. 1–7.

[2] F. Liu et al., "Integrated sensing and communications: Toward dual-functional wireless networks for 6G and beyond," *IEEE Journal on Selected Areas in Communications*, vol. 40, no. 6, pp. 1728–1767, Jun. 2022.

[3] F. Liu, C. Masouros, A. P. Petropulu, H. Griffiths, and L. Hanzo, "Joint Radar and Communication Design: Applications, State-of-the-Art, and the Road Ahead," *IEEE Transactions on Communications*, vol. 68, no. 6, pp. 3834–3862, Jun. 2020.

[4] Z. Du, F. Liu, W. Yuan, C. Masouros, Z. Yuan, and S. Xia, "Integrated Sensing and Communications for V2I Networks: Dynamic Predictive Beamforming for Extended Vehicle Targets," *IEEE Transactions on Wireless Communications*, vol. 22, no. 6, pp. 3612–3627, Jun. 2023.

[5] F. Liu, W. Yuan, C. Masouros, and J. Yuan, "Radar-Assisted Predictive Beamforming for Vehicular Links: Communication Served by Sensing," *IEEE Transactions on Wireless Communications*, vol. 19, no. 11, pp. 7704–7719, Nov. 2020.

[6] X. Meng, F. Liu, W. Yuan, and Q. Zhang, "Sensing Assisted Predictive Beamforming for V2I Networks: Tracking on the Complicated Road : (Invited Paper)," in *23rd International Workshop on Signal Processing Advances in Wireless Communication (SPAWC 2022)*, Oulu, Finland: IEEE, Jul. 2022, pp. 1–5.

[7] F. Liu and C. Masouros, "A Tutorial on Joint Radar and Communication Transmission for Vehicular Networks—Part III: Predictive Beamforming Without State Models," *IEEE Communications Letters*, vol. 25, no. 2, pp. 332–336, Oct. 2021.

[8] Z. Wang, V. W. Wong, and R. Schober, "Integrated Sensing and Communications for End-to-End Predictive Beamforming Design in Vehicle-to-Infrastructure Networks," *IEEE Journal of Selected Topics in Signal Processing*, vol. 18, no. 5, pp. 933–949, 2024.

[9] E. B. Kama, M. B. Salman, I. Skog, and E. Björnson, "Sensing Management for Pilot-Free Predictive Beamforming in Cell-Free Massive MIMO Systems," arXiv, eess.SP 2510.06936, Oct. 2025.

[10] X. Yang, Z. Wei, J. Xu, H. Wu, and Z. Feng, "Cooperative Sensing-Assisted Predictive Beam Tracking for MIMO-OFDM Networked ISAC Systems," *IEEE Transactions on Wireless Communications*, vol. 24, no. 12, pp. 10 660–10 674, Dec. 2025.

[11] Z. He, W. Xu, H. Shen, Y. Huang, and H. Xiao, "Energy Efficient Beamforming Optimization for Integrated Sensing and Communication," *IEEE Wireless Communications Letters*, vol. 11, no. 7, pp. 1374–1378, Jul. 2022.

[12] O. Kanhere, H. Poddar, Y. Xing, D. Shakya, S. Ju, and T. S. Rappaport, "A Power Efficiency Metric for Comparing Energy Consumption in Future Wireless Networks in the Millimeter-Wave and Terahertz Bands," *IEEE Wireless Communications*, vol. 29, no. 6, pp. 56–63, Dec. 2022.

[13] A. Rezaei, A. Khalili, J. Jalali, H. Shafiei, and Q. Wu, "Energy-Efficient Resource Allocation and Antenna Selection for IRS-Assisted Multicell Downlink Networks," *IEEE Wireless Communications Letters*, vol. 11, no. 6, pp. 1229–1233, Jun. 2022.

[14] J. M. Meredith, J. Krause, and P. Merias, "Study on channel model for frequencies from 0.5 to 100 GHz (Release 14)," 3rd Generation Partnership Project (3GPP), 3rd Generation Partnership Project (3GPP), Sophia Antipolis, France, Technical Report (TR) TR 38.901, Mar. 2017. [Online]. Available: https://3gpp.org.

[15] O. Arnold, F. Richter, G. P. Fettweis, and O. Blume, "Power consumption modeling of different base station types in heterogeneous cellular networks," in *19th Future Network & Mobile Summit (FutureNetw 2010)*, Florence, Italy: IEEE, Jun. 2010, pp. 1–8.

[16] W. Dinkelbach, "On Nonlinear Fractional Programming," *Management Science*, vol. 13, no. 7, pp. 492–498, Mar. 1967.

[17] G. Scutari and Y. Sun, *Parallel and Distributed Successive Convex Approximation Methods for Big-Data Optimization* (Lecture Notes in Mathematics), 1st ed. Springer, Cham., 2018, vol. 2224.

[18] S. Boyd and L. Vandenberghe, *Convex optimization*. Cambridge University Press, 2004.